

A Nested Variational Time Discretization for Parametric Anisotropic Willmore Flow

Ricardo Perl
Paola Pozzi
Martin Rumpf

Abstract

A variational time discretization of anisotropic Willmore flow combined with a spatial discretization via piecewise affine finite elements is presented. Here, both the energy and the metric underlying the gradient flow are anisotropic, which in particular ensures that Wulff shapes are invariant up to scaling under the gradient flow. In each time step of the gradient flow a nested optimization problem has to be solved. Thereby, an outer variational problem reflects the time discretization of the actual Willmore flow and involves an approximate anisotropic L^2 -distance between two consecutive time steps and a fully implicit approximation of the anisotropic Willmore energy. The anisotropic mean curvature needed to evaluate the energy integrand is replaced by the time discrete, approximate speed from an inner, fully implicit variational scheme for anisotropic mean curvature motion. To solve the nested optimization problem a Newton method for the associated Lagrangian is applied. Computational results for the evolution of curves underline the robustness of the new scheme, in particular with respect to large time steps.

1 Introduction

This paper generalizes a recently proposed variational time discretization [1] for isotropic Willmore flow to the corresponding anisotropic flow. Thereby, the anisotropic Willmore flow is defined as the gradient flow of the anisotropic Willmore energy with respect to the corresponding anisotropic L^2 -metric.

The isotropic Willmore energy is given by $w[x] = \frac{1}{2} \int_{\mathcal{M}} \mathbf{h}^2 da$, where x denotes the identity map and \mathbf{h} the mean curvature on a surface \mathcal{M} . The isotropic L^2 -metric is given by $(v, v)_{\mathcal{M}} = \int_{\mathcal{M}} |v|^2 da$, which is considered as a squared L^2 -distance of the surface \mathcal{M} being displaced with the vector field v from the non displaced surface \mathcal{M} . In the hypersurface case Willmore flow leads to a fourth order parabolic evolution problem, which defines for a given initial surface \mathcal{M}_0 a family of surfaces $\mathcal{M}(t)$ for $t \geq 0$ with $\mathcal{M}(0) = \mathcal{M}_0$ [49, 47, 30]. Applications of a minimization of the isotropic Willmore energy and the corresponding Willmore flow include the processing of edge sets in imaging [36, 34, 51, 13], geometry processing [48, 9, 8, 50] and the mathematical treatment of biological membranes [29, 46, 24]. Starting with work by Polden [40, 41] existence and regularity of Willmore flow was advanced in the last decade [33, 31, 43].

Now, in the context of Finsler geometry the classical area functional is replaced by the anisotropic area functional $\mathbf{a}_{\gamma}[x] = \int_{\mathcal{M}} \gamma(n) da$ with a local area weight $\gamma(n)$ depending on the

local surface orientation. Here, γ is a positive, 1-homogeneous anisotropy function. In analogy to the isotropic case the anisotropic mean curvature \mathbf{h}_γ is defined as the L^2 -representation of the variation of the anisotropic area in the direction of normal variations of the surface and can be evaluated as $\mathbf{h}_\gamma = \operatorname{div}_{\mathcal{M}}(\nabla\gamma(n))$. Hence, a possible first choice for an anisotropic Willmore functional is given by $\frac{1}{2} \int_{\mathcal{M}} \mathbf{h}_\gamma^2 da$. Clarenz [15] has shown that Wulff shapes are the only minimizers of this energy. Palmer [39] studied variational problems involving anisotropic bending energies for surfaces with and without boundaries. Unfortunately, this energy definition does not imply the scale invariance property of Wulff shapes known for round spheres under isotropic Willmore flow. Indeed, any round sphere is a stationary point of the isotropic Willmore functional in \mathbb{R}^3 . In \mathbb{R}^2 a circle of radius R_0 evolves under isotropic Willmore flow according to the ordinary differential equation $\dot{R} = \frac{1}{2}R^{-3}$. The counterpart of a round sphere in the anisotropic context is the Wulff shape as the unit ball with respect to the norm associated with the dual γ^* of the anisotropy γ . But there is no such scaling law for the evolution of Wulff shapes under the above anisotropic variant of Willmore flow.

To ensure full consistency with the Finsler geometry, one has to adapt both the anisotropic energy and the anisotropic metric as suggested in [42] (see Section 2). Indeed, we make use of the associated anisotropic metric $\int_{\mathcal{M}} \gamma^*(v)(\nabla\gamma^*)(v) \cdot v \gamma(n) da$ (here only defined for $v(x) \neq 0$ for all $x \in \mathcal{M}$, cf. Section 3 for the general case), acting on a motion field v of the surface \mathcal{M} with normal n . Furthermore, we will use the anisotropic area weight to define the anisotropic Willmore energy, i.e. $w_\gamma(x) = \frac{1}{2} \int_{\mathcal{M}} \mathbf{h}_\gamma^2 \gamma(n) da$. Then, it actually turned out that Wulff shapes in \mathbb{R}^2 actually evolve according to the same evolution law for radial parameter valid for the evolution of circles under the isotropic flow. Recently, Bellettini & Mugnai [7] investigated the first variation of this functional in the smooth case. Concerning the proper time and space discretization, this consistent choice of the anisotropic Willmore energy and the anisotropic metric on surface variations perfectly fits to the framework of the natural variational time discretization of geometric gradient flows.

The finite element approximation of Willmore flow was first investigated by Rusu [44] based on a mixed method for the surface parametrization x and the mean curvature vector $\mathbf{h}n$ as independent variables, see also [16] for the application to surface restoration. In [23] a level set formulation of Willmore flow was proposed. In the case of graph surfaces Deckelnick and Dziuk [18] were able to prove convergence of a related space discrete and time continuous scheme. Deckelnick and Schieweck established convergence of a conforming finite element approximation for axial symmetric surfaces [20]. In the case of the elastic flow of curves an error analysis was given by Dziuk and Deckelnick in [19]. An alternative scheme, which in particular ensures a better distribution of nodes on the evolving surface was presented by Barrett, Garcke and Nürnberg [2, 4]. Using discrete geometry calculus Bobenko and Schröder [10] suggested a discrete Willmore flow of triangular surfaces. The time discretization of the second order, anisotropic mean curvature flow has been considered by Dziuk already in [27, 28] and he gave convergence results for curves. Diewald [21] has extended the discretization approach for isotropic Willmore flow of Rusu [44] to some anisotropic variant, for which Droske [22] and Nemitz [35] investigated a level set discretization.

Most of the above discretization methods are based on some semi-implicit time discretization, which requires the solution of linear systems of equations at each time step. Thereby, the involved geometric differential operators are assembled on the surface from the previous time step. In the application one observes strong restrictions on the time step size. This shortcoming motivated the development of a new approach for the time discretization of Willmore flow in [1] based on the following general concept for a variational time discretization of gradient flows: The gradient flow on a (in general infinite dimensional) manifold with respect to an en-

ergy $e[\cdot]$ and a metric g on the manifold, is defined as the evolution problem $\dot{x} = -\text{grad}_g e[x]$ with initial data x^0 , where $\text{grad}_g e[x]$ is the representation of the variation $e'[x]$ in the metric g , i.e. $g(\text{grad}_g e[x], \zeta) = e'[x](\zeta)$ for all infinitesimal variations ζ of x . Now, one defines a time discrete family $(x^k)_{k=0, \dots}$ with the desired property $x^k \approx x(k\tau)$ for the given time step size τ . To this end, one successively solves a sequence of variational problems, i.e. in time step k

$$x^{k+1} = \arg \min_x \text{dist}(x^k, x)^2 + 2\tau e[x],$$

where $\text{dist}(x^k, x) = \inf_{\gamma \in \Gamma[x^k, x]} \int_0^1 \sqrt{g_{\gamma(s)}(\dot{\gamma}(s), \dot{\gamma}(s))} ds$ denotes the Riemannian distance of x from x^k on the manifold and $\Gamma[x^k, x]$ is the set of smooth curves γ with $\gamma(0) = x^k$ and $\gamma(1) = x$. The striking observation for this abstract scheme is that one immediately obtains an energy estimate, i.e. $e[x^{k+1}] + \frac{1}{2\tau} \text{dist}(x^k, x^{k+1})^2 \leq e[x^k]$. In the context of geometric flows, this approach was studied by Luckhaus and Sturzenhecker [32] leading to a fully implicit variational time discretization for mean curvature motion in BV and by Chambolle [11], who reformulated this scheme in terms of a level set method and generalized it for the approximation of anisotropic mean curvature motion in [6, 12]. The time discretization for Willmore flow proposed in [1] builds upon this general paradigm. In this paper, we will show how to adapt the approach to the time discretization of the anisotropic Willmore flow which is fully consistent with Finsler geometry.

The paper is organized as follows. In Section 2 we briefly review the time discretization of isotropic Willmore flow. Building on these prerequisites the generalization to anisotropic Willmore flow is discussed in Section 3. Then, in Section 4 we discuss a fully discrete numerical scheme based on piecewise affine finite elements on simplicial surface meshes. In Section 5 the Lagrangian calculus from PDE constraint optimization is used to develop a suitable algorithm for the solution of the nested optimization problem to be solved in each time step. Finally, in Section 6 computational results are presented. An appendix collects essential ingredients of the corresponding algorithm.

2 Review of the time discretization of isotropic Willmore flow

In this section we will briefly recall the nested time discretization of isotropic Willmore from [1]. We denote a hypersurface in \mathbb{R}^{d+1} by $\mathcal{M} = \mathcal{M}[y]$. Here, y indicates a parametrization of \mathcal{M} and can also be considered as the identity map on \mathcal{M} parametrizing \mathcal{M} over itself. Then, the abstract variational time discretization of isotropic Willmore flow reads as follows:

For given surface $\mathcal{M}[x^k]$ with parametrization x^k and a time step τ find a mapping $x = x[x^k]$ such that $\text{dist}(\mathcal{M}[x^k], \mathcal{M}[x])^2 + \tau \int_{\mathcal{M}[x]} \mathbf{h}^2 da \rightarrow \min$, where

$\text{dist}(\mathcal{M}[z], \mathcal{M}[v])^2 = \int_{\mathcal{M}[z]} (v - z)^2 da$ is the squared L^2 -distance of surfaces $\mathcal{M}[v]$ from the surface $\mathcal{M}[z]$, $\mathbf{h} = \mathbf{h}[x]$ is the mean curvature of $\mathcal{M}[x]$, and $\int_{\mathcal{M}[x]} da$ denotes the surface area of $\mathcal{M}[x]$. Now, we take into account that the mean curvature $\mathbf{h} = \mathbf{h}[x]$ is the L^2 -gradient of the area functional on a surface $\mathcal{M}[x]$ and that mean curvature motion is the corresponding gradient flow. Thus, the mean curvature vector $\mathbf{h}[x]n[x]$ with $n = n[x]$ denoting the normal on $\mathcal{M}[x]$ can be approximated by the discrete time derivative $\frac{y[x] - x}{\tilde{\tau}}$, where $y[x]$ is a suitable approximation of a single time step of the evolution of mean curvature motion with initial data x and time step size $\tilde{\tau}$. This time step itself can again be approximated using an (inner) variational scheme, i.e.

we define $y[x]$ to be the minimizer of

$$e_{\text{in}}[x, y] := \int_{\mathcal{M}[x]} (y - x)^2 + \tilde{\tau} |\nabla_{\mathcal{M}[x]} y|^2 da. \quad (2.1)$$

In fact, the corresponding Euler Lagrange equation is identical to the defining equation of the semi-implicit scheme for mean curvature motion proposed by Dziuk [26]:

$$0 = \int_{\mathcal{M}[x]} (y - x)\theta + \tilde{\tau} \nabla_{\mathcal{M}[x]} y \cdot \nabla_{\mathcal{M}[x]} \theta da \quad (2.2)$$

Now, given $y[x]$ as the minimizer of (2.1) for small $\tilde{\tau}$ the functional $\frac{1}{2} \int_{\mathcal{M}[x]} \frac{(y[x]-x)^2}{\tilde{\tau}^2} da$ is an approximation of the Willmore functional on $\mathcal{M}[x]$. This approximation is then used to define a variational scheme for a time step of the actual Willmore flow. To this end, we consider for given surface parametrization x^k the functional

$$e_{\text{out}}[x^k, x, y] := \int_{\mathcal{M}[x^k]} (x - x^k)^2 da + \frac{\tau}{\tilde{\tau}^2} \int_{\mathcal{M}[x]} (y - x)^2 da,$$

where we suppose $y = y[x]$ to be the minimizer of (2.1). To summarize, we obtain the following scheme for the k th time step of Willmore flow:

Given an initial surface $\mathcal{M}[x^0]$ with parametrization x^0 we define a sequence of surfaces $\mathcal{M}[x^k]$ with parametrizations x^k for $k = 1, \dots$ via the solution of the following sequence of nested variational problems

$$x^{k+1} = \arg \min_x e_{\text{out}}[x^k, x, y[x]], \text{ where} \quad (2.3)$$

$$y[x] = \arg \min_y e_{\text{in}}[x, y]. \quad (2.4)$$

The inner variational problem (2.4) is quadratic, thus the resulting Euler–Lagrange equation (2.2) is linear and we end up with a PDE constrained optimization problem to be solved in each time step. For more details we refer to [1].

3 Nested time discretization for anisotropic Willmore flow

Now, let us investigate the time discretization of anisotropic Willmore flow in the co-dimension one case. Here, we will in particular focus on the proper choice of energy and metric. We assume that $\gamma : \mathbb{R}^{d+1} \rightarrow [0, \infty)$ is a positive, 1-homogeneous (i.e. $\gamma(\lambda p) = |\lambda| \gamma(p)$ for all $\lambda \in \mathbb{R}, p \in \mathbb{R}^{d+1}$) and sufficiently regular function, that satisfies the ellipticity condition

$$\gamma''(p)qq \geq c_0 \|q\|^2 \quad \forall p, q \in \mathbb{R}^{d+1}, \|p\| = 1, p \cdot q = 0 \quad (3.1)$$

for some positive constant c_0 and the Euclidean norm $\|\cdot\|$. As already mentioned $\gamma(n)$ represents the anisotropic area weight for a surface normal n . The isotropic case is recovered by choosing $\gamma(\cdot) = \|\cdot\|$. We define the dual function of γ as

$$\gamma^*(x) := \sup\{\langle x, \psi \rangle \mid \psi \in B_\gamma\} \quad \forall x \in \mathbb{R}^{d+1},$$

where B_γ denotes the unit Ball in the γ -norm. The ellipticity assumption ensures that $(\mathbb{R}^{d+1}, \gamma)$ and its dual space $(\mathbb{R}^{d+1}, \gamma^*)$ are uniformly convex Banach spaces and the duality map $T : (\mathbb{R}^{d+1}, \gamma^*) \rightarrow (\mathbb{R}^{d+1}, \gamma)$, with

$$T(x) = \frac{1}{2} \partial(\gamma^*(x)^2),$$

is an odd single-valued bijective continuous map. More precisely $T(0) = 0$, $T(x) = \gamma^*(x) \nabla \gamma^*(x)$ for $x \neq 0$, and $T^{-1}(\xi) = \gamma(\xi) \nabla \gamma(\xi)$ for $\xi \neq 0$. For details we refer to [42]. The unit ball $\mathcal{F} := \{x \in \mathbb{R}^{d+1} : \gamma(x) \leq 1\}$ in $(\mathbb{R}^{d+1}, \gamma)$ is denoted the Frank diagram, the associated dual unit ball $\mathcal{W} := \{x \in \mathbb{R}^{d+1} : \gamma^*(x) \leq 1\}$ is the corresponding Wulff shape. Wulff shapes are known to be solutions to the isoperimetric problem, that is $\partial \mathcal{W}$ minimizes the anisotropic area functional

$$\mathbf{a}_\gamma[x] = \int_{\mathcal{M}[x]} \gamma(n[x]) da \quad (3.2)$$

(with $\gamma(n[x]) da$ denoting the anisotropic area element) in the class of surfaces enclosing the same volume (cf. [17] and the references therein). Now, based on the anisotropy γ and its dual γ^* we define an anisotropic distance dist_γ of a manifold $\mathcal{M}[y]$ from a manifold $\mathcal{M}[x]$ by

$$\text{dist}_\gamma(\mathcal{M}[x], \mathcal{M}[y])^2 := \int_{\mathcal{M}[x]} \gamma^*(y-x)^2 \gamma(n[x]) da \quad (3.3)$$

for sufficiently regular x and y . The choice of the norm γ^* together with the anisotropic area weight $\gamma(n[x])$ in (3.3) reflects the fact that the anisotropic area of the boundary of a convex body $K \subset \mathbb{R}^{d+1}$ can be interpreted as

$$\mathbf{a}_\gamma(\partial K) = \lim_{\epsilon \rightarrow 0} \frac{|K + \epsilon \mathcal{W}| - |K|}{\epsilon},$$

where $|\cdot|$ denotes the usual Lebesgue volume in \mathbb{R}^{d+1} . In particular, the underlying metric structure is dictated by the Wulff shape and its norm γ^* (see [5], [42] and references therein).

Based on these considerations let us first consider anisotropic mean curvature motion, which is defined as the gradient flow of the anisotropic surface area with respect to the above anisotropic metric. In this case the variational time discretization is associated with the minimization of

$$\text{dist}_\gamma(\mathcal{M}[x], \mathcal{M}[y])^2 + 2\tilde{\tau} \int_{\mathcal{M}[y]} \gamma(n[y]) da \quad (3.4)$$

with respect to y for a given surface $\mathcal{M}[x]$ and $\tilde{\tau} > 0$. Let us denote by $y[x]$ the minimizer for given surface parameterization x . The Euler Lagrange equation for (3.4) is given by

$$\begin{aligned} 0 &= \int_{\mathcal{M}[x]} T(y-x) \cdot \theta \gamma(n[x]) da + \tilde{\tau} \langle a'_\gamma[y], \theta \rangle \\ &= \tilde{\tau} \int_{\mathcal{M}[x]} T\left(\frac{y-x}{\tilde{\tau}}\right) \cdot \theta \gamma(n[x]) da + \tilde{\tau} \langle a'_\gamma[y], \theta \rangle \end{aligned} \quad (3.5)$$

for smooth test functions $\theta : \mathcal{M}[x] \rightarrow \mathbb{R}^{d+1}$. Together with $\partial_t y(k\tilde{\tau}) \approx \frac{y-x}{\tilde{\tau}}$ this reflects the weak formulation of anisotropic mean curvature motion given by

$$\int_{\mathcal{M}[y]} T(\partial_t y) \cdot \theta \gamma(n[y]) da = -\langle \mathbf{a}_\gamma'[y], \theta \rangle \quad (3.6)$$

for a parametrization y and smooth test functions θ defined on $\mathcal{M}[y]$ (cf. [42]). Here, the variation of the anisotropic area functional is given by

$$\langle \mathbf{a}_\gamma'[y], \theta \rangle = \int_{\mathcal{M}[y]} \mathbf{h}_\gamma[y] \frac{n[y]}{\gamma(n[y])} \cdot \theta \gamma(n[y]) da,$$

where $\mathbf{h}_\gamma[y] = \operatorname{div}_{\mathcal{M}[y]}(n_\gamma[y]) = \operatorname{div}_{\mathcal{M}[y]}(\nabla \gamma(n[y]))$ denotes the anisotropic mean curvature with $n_\gamma[y] = \nabla \gamma(n[y])$ (see [14]). Thus, from (3.6) we deduce that $T(\partial_t y) = -\mathbf{h}_\gamma[y] \frac{n[y]}{\gamma(n[y])}$ or equivalently we achieve the strong formulation of anisotropic mean curvature motion

$$\partial_t y = \kappa_\gamma[y] := T^{-1} \left(-\mathbf{h}_\gamma[y] \frac{n[y]}{\gamma(n[y])} \right) = -\mathbf{h}_\gamma[y] \nabla \gamma(n[y]).$$

Indeed, as pointed out in [42] the last equality holds due to the 1-homogeneity of γ , i.e.

$$\begin{aligned} \gamma \left(-\mathbf{h}_\gamma[y] \frac{n[y]}{\gamma(n[y])} \right) \nabla \gamma \left(-\mathbf{h}_\gamma[y] \frac{n[y]}{\gamma(n[y])} \right) &= -\frac{\mathbf{h}_\gamma[y]}{\gamma(n[y])} \gamma(n[y]) \nabla \gamma(n[y]) \\ &= -\mathbf{h}_\gamma[y] \nabla \gamma(n[y]). \end{aligned}$$

Next, we deal with the actual anisotropic Willmore flow and consider the anisotropic Willmore functional defined as follows for a parametrization x of $\mathcal{M}[x]$:

$$w_\gamma[x] := \frac{1}{2} \int_{\mathcal{M}[x]} \mathbf{h}_\gamma[x]^2 \gamma(n[x]) da = \frac{1}{2} \int_{\mathcal{M}[x]} \gamma^*(\kappa_\gamma[x])^2 \gamma(n[x]) da. \quad (3.7)$$

Here, we have used that the 1-homogeneity and $\nabla \gamma(\xi) \in \partial \mathcal{W}$ for all $\xi \in \mathbb{R}^{d+1}$ imply

$$\gamma^*(\kappa_\gamma)^2 = \gamma^*(-\mathbf{h}_\gamma \nabla \gamma(n))^2 = \mathbf{h}_\gamma^2 \gamma^*(-\nabla \gamma(n))^2 = \mathbf{h}_\gamma^2.$$

Then the abstract variational time discretization of anisotropic Willmore flow reads as follows:

Given $\mathcal{M}[x^k]$ and time step τ find a mapping $x = x[x^k]$ such that x minimizes

$$\operatorname{dist}_\gamma(\mathcal{M}[x^k], \mathcal{M}[x])^2 + \tau \int_{\mathcal{M}[x]} \gamma^*(\kappa_\gamma[x])^2 \gamma(n[x]) da. \quad (3.8)$$

As in the isotropic case, we will now replace the anisotropic mean curvature vector by the discrete speed extracted from a scheme for a single time step of anisotropic curvature flow (3.6). In explicit, $\gamma^*(\frac{y[x]-x}{\tilde{\tau}})^2$ is a suitable approximation of $\mathbf{h}_\gamma^2[x] = \gamma^*(\kappa_\gamma[x])^2$, where $\frac{y[x]-x}{\tilde{\tau}}$ is the time discrete speed extracted from the variational time discretization of anisotropic curvature motion. Furthermore, we use the definition of the anisotropic distance measure in (3.3). Finally, based on this approximation we derive the actual time discretization of anisotropic Willmore flow. For a given surface parametrization x^k of the surface $\mathcal{M}[x^k]$ at a time step k we define the functionals

$$\begin{aligned} e_{\text{out}}[x^k, x, y] &:= \int_{\mathcal{M}[x^k]} \gamma^*(x - x^k)^2 \gamma(n[x^k]) da + \frac{\tau}{\tilde{\tau}^2} \int_{\mathcal{M}[x]} \gamma^*(y - x)^2 \gamma(n[x]) da, \\ e_{\text{in}}[x, y] &:= \int_{\mathcal{M}[x]} \gamma^*(y - x)^2 \gamma(n[x]) da + 2\tilde{\tau} \int_{\mathcal{M}[y]} \gamma(n[y]) da, \end{aligned}$$

and in analogy to the isotropic case above, we end up with the following fully nonlinear variational time discretization of anisotropic Willmore flow:

Given an initial surface $\mathcal{M}[x^0]$ with parametrization x^0 we define a sequence of surfaces $\mathcal{M}[x^k]$ with parametrizations x^k for $k = 1, \dots$ via the solution of the following sequence of nested variational problems

$$x^{k+1} = \arg \min_x e_{out}[x^k, x, y[x]], \quad \text{where} \quad (3.9)$$

$$y[x] = \arg \min_y e_{in}[x, y]. \quad (3.10)$$

Different from the variational scheme for isotropic Willmore flow, the inner variational problem is no longer quadratic. It is worth to mention that this variational time discretization does not involve derivatives of the anisotropy. Nevertheless, as we will discuss below in the context of the actual computation, differentiation is required to run Newton methods for the associated Lagrangian functional. Indeed, for this we will need $\gamma, \gamma^* \in C^3(\mathbb{R}^{d+1} \setminus \{0\})$; moreover, unless $(\gamma^*)^2 \in C^3(\mathbb{R}^{d+1})$ (which holds for $\gamma(p) = \sqrt{Ap \cdot p}$ with a symmetric positive definite matrix A), a regularization will be required (see Section 6 below).

Let us conclude this section with a study of boundaries $\partial\mathcal{W}$ of two-dimensional Wulff shapes \mathcal{W} moving under anisotropic Willmore flow in the plane. To this end consider the parametrization $x : (0, T) \times S^1 \rightarrow \mathbb{R}^2$, $x(t, \nu) = R(t)\nabla\gamma(\nu)$ of the boundary of a (rescaled) Wulff shape $R(t)\mathcal{W}$. Using the results given in [42] it is easily seen that x moves under anisotropic Willmore flow if $R(t)$ solves the ODE

$$\dot{R}(t) = \frac{1}{2R(t)^3}.$$

Hence, we observe that Wulff shapes expand in time like in the isotropic case (cf. [1]) with $R(t) = \sqrt[4]{R(0)^4 + 2t}$. Next let us compare this with the time discrete evolution based on the proposed nested variational time discretization. We write $x, y, x^k : S^1 \rightarrow \mathbb{R}^2$, $x(\nu) = R\nabla\gamma(\nu)$, $y(\nu) = \tilde{R}\nabla\gamma(\nu)$, $x^k(\nu) = R^k\nabla\gamma(\nu)$. Since $\gamma^*(\nabla\gamma(\nu)) = 1$ we immediately derive

$$\begin{aligned} e_{out}[x^k, x, y] &= (R - R^k)^2 \mathbf{a}_\gamma(x^k) + \frac{\tau}{\tilde{\tau}^2} (\tilde{R} - R)^2 \mathbf{a}_\gamma(x), \\ e_{in}[x, y] &= (\tilde{R} - R)^2 \mathbf{a}_\gamma(x) + 2\tilde{\tau} \mathbf{a}_\gamma(y). \end{aligned}$$

Considering variations $y_\epsilon(\nu) = (\tilde{R} + \epsilon\psi)\nabla\gamma(\nu)$ in direction of the anisotropic normal n_γ we infer from the inner problem that

$$(\tilde{R} - R)\mathbf{a}_\gamma(x) + \frac{\tilde{\tau}}{\tilde{R}}\mathbf{a}_\gamma(y) = 0.$$

More precisely, since $\mathbf{a}_\gamma(y) = \frac{\tilde{R}}{R}\mathbf{a}_\gamma(x)$ due to the homogeneity property of γ , we have that

$$\tilde{R} = R - \frac{\tilde{\tau}}{R}.$$

This, together with $\mathbf{a}_\gamma(x) = \frac{R}{R^k}\mathbf{a}_\gamma(x^k)$, gives

$$e_{out}[x^k, x, y] = \mathbf{a}_\gamma(x^k) \left((R - R^k)^2 + \frac{\tau}{RR^k} \right),$$

from which we deduce

$$\frac{R - R^k}{\tau} = \frac{1}{2R^k R^2}.$$

Note that this is a slightly different time step scheme than the one reported for the isotropic case ($\gamma(\cdot) = \|\cdot\|$) in [1, § 2.1]. This is due to fact that we use an implicit formulation of the inner problem as opposed to the linear equation (2.1) in the scheme for isotropic Willmore flow (cf. Section 2).

4 Finite element discretization in space

Following the approach in [1] we now derive a suitable spatial discretization based on piecewise affine finite elements. This is in close correspondence to the surface finite element approach by Dziuk [25]. To this end we consider simplicial meshes $\mathcal{M}[X]$ as approximations of the hypersurfaces $\mathcal{M}[x]$ in \mathbb{R}^{d+1} , i.e. polygonal curves for $d = 1$ and triangular surfaces for $d = 2$. Thereby, X is a parametrization of the simplicial mesh $\mathcal{M}[X]$ which is uniquely described by a vector \bar{X} of vertex positions of the mesh. Here, and in what follows, we will always denote discrete quantities with upper case letters to distinguish them from the corresponding continuous quantities in lower case letters. Furthermore, a bar on top of a discrete function indicates the associated vector of nodal values, i.e. $\bar{X} = (\bar{X}_i)_{i \in I}$, where $\bar{X}_i = (X_i^1, \dots, X_i^{d+1})$ is the coordinate vector of the i th vertex of the mesh and I denotes the index set of vertices. For $d = 1$ each element T is a line segment with nodes X_0 and X_1 (using local indices) and for $d = 2$ the elements T are planar triangles with vertices X_0, X_1 , and X_2 and edge vectors $F_0 = X_2 - X_1, F_1 = X_0 - X_2$, and $F_2 = X_1 - X_0$. Given a simplicial surface $\mathcal{M}[X]$, the associated piecewise affine finite element space is given by

$$\mathcal{V}(\mathcal{M}[X]) := \{U \in C^0(\mathcal{M}[X]) \mid U|_T \in \mathcal{P}_1 \forall T \in \mathcal{M}[X]\}$$

with the nodal basis denoted by $\{\Phi_i\}_{i \in I}$. Here, \mathcal{P}_1 is the space of affine functions on a simplex T . Thus, for $U \in \mathcal{V}(\mathcal{M}[X])$ we obtain $U = \sum_{i \in I} U(X_i) \Phi_i$ and $\bar{U} = (U(X_i))_{i \in I}$. Let us emphasize, that the parametrization mapping X itself is considered as an element in $\mathcal{V}(\mathcal{M}[X])^{d+1}$ and we recover the vector of nodes $\bar{X} = (X_i)_{i \in I}$.

With these algorithmic ingredients at hand we now can derive a fully discrete nested time discretization of anisotropic Willmore flow, as the spatially discrete counterpart of (3.9) and (3.10):

Given a discrete initial surface $\mathcal{M}[X^0]$ with discrete parametrization X^0 we compute a sequence of surfaces $\mathcal{M}[X^k]$ with parametrizations X^k by solving the nested, finite dimensional variational problems

$$X^{k+1} = \arg \min_{X \in \mathcal{V}(\mathcal{M}[X^k])^{d+1}} \mathcal{E}_{\text{out}}[X^k, X, Y[X]], \quad \text{where,} \quad (4.1)$$

$$Y[X] = \arg \min_{Y \in \mathcal{V}(\mathcal{M}[X])^{d+1}} \mathcal{E}_{\text{in}}[X, Y]. \quad (4.2)$$

Here, the functionals \mathcal{E}_{in} and \mathcal{E}_{out} are straightforward spatially discrete counterpart of the functionals $e_{\text{in}}[x, y]$ and $e_{\text{out}}[x^k, x, y]$ and defined by

$$\begin{aligned} \mathcal{E}_{\text{in}}[X, Y] &:= \int_{\mathcal{M}[X]} \mathbf{I}(\gamma^*(Y - X)^2) \gamma(N[X]) da + 2\tilde{\tau} \int_{\mathcal{M}[Y]} \gamma(N[Y]) da, \\ \mathcal{E}_{\text{out}}[X^k, X, Y] &:= \int_{\mathcal{M}[X^k]} \mathbf{I}(\gamma^*(X - X^k)^2) \gamma(N[X^k]) da \\ &\quad + \frac{\tau}{\tilde{\tau}^2} \int_{\mathcal{M}[X]} \mathbf{I}(\gamma^*(Y - X)^2) \gamma(N[X]) da, \end{aligned}$$

where the nodal interpolation operator \mathbf{I} renders the resulting scheme fully practical. To simplify the exposition, we introduce the discrete quadratic form $\mathbf{M}_\gamma[Z, X] = \int_{\mathcal{M}[X]} \mathbf{I}(\gamma^*(Z)^2) \gamma(N[X]) da$ (a nonlinear counter part of the quadratic form induced by the lumped mass matrix) and the discrete anisotropic area functional $\mathbf{A}_\gamma[Y] = \int_{\mathcal{M}[Y]} \gamma(N[Y]) da$, both of which are assembled from local contributions on simplices of the underlying simplicial grid \mathcal{T}_h :

$$\mathbf{M}_\gamma[Z, X] = \sum_{T \in \mathcal{T}_h} \frac{1}{(d+1)!} \left(\sum_{i=0, \dots, d} \gamma^*(\bar{Z}_{T,i})^2 \right) \gamma(R_T[\bar{X}]) \quad (4.3)$$

$$\mathbf{A}_\gamma[X] = \sum_{T \in \mathcal{T}_h} \frac{1}{d!} \gamma(R_T[\bar{X}]) \quad (4.4)$$

Here, $R_T[\bar{X}] = D^{90}(\bar{X}_{T,1} - \bar{X}_{T,0})$ for $d = 1$ and $R_T[\bar{X}] = (\bar{X}_{T,1} - \bar{X}_{T,0}) \wedge (\bar{X}_{T,2} - \bar{X}_{T,0})$ for $d = 2$. Hence, we can rewrite

$$\begin{aligned} \mathcal{E}_{\text{out}}[X^k, X, Y] &= \mathbf{M}_\gamma[X - X^k, X^k] + \frac{\tau}{\tilde{\tau}^2} \mathbf{M}_\gamma[Y - X, X], \\ \mathcal{E}_{\text{in}}[X, Y] &= \mathbf{M}_\gamma[Y - X, X] + 2\tilde{\tau} \mathbf{A}_\gamma[Y]. \end{aligned}$$

The necessary condition for $Y[X]$ to be a minimizer of $\mathcal{E}_{\text{in}}[X, \cdot]$ is given by the corresponding discrete Euler Lagrange equation

$$0 = \partial_Y \mathcal{E}_{\text{in}}[X, Y[X]](\Theta) = \partial_Z \mathbf{M}_\gamma[Y - X, X](\Theta) + 2\tilde{\tau} \partial_Y \mathbf{A}_\gamma[Y](\Theta)$$

for all $\Theta \in \mathcal{V}(\mathcal{M}[X])^{d+1}$.

5 Optimization algorithm for the time steps

In this section, the actual optimization algorithm for the nested, fully discrete variational problem derived in Section 4 is presented. Thereby, we apply a step size controlled Newton method (cf. [45] section 7) for the corresponding Lagrangian (cf. Nocedal & Wright [37]). In our context the Lagrangian function for problem (4.1), (4.2) is given by

$$\mathcal{L}[\bar{X}, \bar{Y}, \bar{P}] = \mathcal{E}_{\text{out}}[X^k, X, Y] - \partial_Y \mathcal{E}_{\text{in}}[X, Y](P)$$

for independent unknowns $\bar{X}, \bar{Y} \in \mathbb{R}^{(d+1)|I|}$ and the Lagrange multiplier $\bar{P} \in \mathbb{R}^{(d+1)|I|}$ (with a slight misuse of notation, we consider these unknowns as finite element function in the spaces $\mathcal{V}(\mathcal{M}[X^k])^{d+1}$ and $\mathcal{V}(\mathcal{M}[X])^{d+1}$, respectively, or as the associated nodal vector in $\mathbb{R}^{(d+1)|I|}$). For an extensive discussion of the Lagrangian ansatz we refer to [38]. Now, we ask for critical points $(\bar{X}, \bar{Y}, \bar{P})$ of L . Indeed, $0 = \partial_{\bar{P}} \mathcal{L}[\bar{X}, \bar{Y}, \bar{P}](\bar{\Theta}) = -\partial_Y \mathcal{E}_{\text{in}}[X, Y](\Theta)$ is the Euler Lagrange equation of the inner minimization problem with respect to Y for given X and $0 = \partial_{\bar{Y}} \mathcal{L}[\bar{X}, \bar{Y}, \bar{P}](\bar{\Theta}) = \partial_Y \mathcal{E}_{\text{out}}[X^k, X, Y](\Theta) - \partial_Y^2 \mathcal{E}_{\text{in}}[X, Y](P, \Theta)$ is the defining equation for the dual solution P given Y as the solution of the above Euler Lagrange equation. Finally, the Euler Lagrange equation for the actual constraint optimization problem coincides with

$$0 = \partial_{\bar{X}} \mathcal{L}[\bar{X}, \bar{Y}, \bar{P}](\bar{\Theta}) = \partial_X \mathcal{E}_{\text{out}}[X^k, X, Y](\Theta) - \partial_X \partial_Y \mathcal{E}_{\text{in}}[X, Y](P, \Theta).$$

For the gradient of the Lagrangian \mathcal{L} we obtain

$$\text{grad } \mathcal{L} = \begin{pmatrix} \partial_X \mathcal{E}_{\text{out}} - \partial_X \partial_Y \mathcal{E}_{\text{in}}(P) \\ \partial_Y \mathcal{E}_{\text{out}} - \partial_Y^2 \mathcal{E}_{\text{in}}(P) \\ -\partial_Y \mathcal{E}_{\text{in}} \end{pmatrix}$$

with

$$\begin{aligned} \partial_X \mathcal{E}_{\text{out}}[X^k, X, Y](\Theta) &= \partial_Z \mathbf{M}_\gamma[X - X^k, X^k](\Theta) \\ &\quad + \frac{\tau}{\tilde{\tau}^2} (\partial_X \mathbf{M}_\gamma[Y - X, X](\Theta) - \partial_Z \mathbf{M}_\gamma[Y - X, X](\Theta)), \\ \partial_Y \mathcal{E}_{\text{out}}[X^k, X, Y](\Theta) &= \frac{\tau}{\tilde{\tau}^2} \partial_Z \mathbf{M}_\gamma[Y - X, X](\Theta), \end{aligned}$$

$$\begin{aligned}\partial_X \partial_Y \mathcal{E}_{\text{in}}[X, Y](P, \Theta) &= -\partial_Z^2 \mathbf{M}_\gamma[Y - X, X](P, \Theta) + \partial_X \partial_Z \mathbf{M}_\gamma[Y - X, X](P, \Theta), \\ \partial_Y^2 \mathcal{E}_{\text{in}}[X, Y](P, \Theta) &= \partial_Z^2 \mathbf{M}_\gamma[Y - X, X](P, \Theta) + 2\tilde{\tau} \partial_Y^2 \mathbf{A}_\gamma[Y](P, \Theta).\end{aligned}$$

The Hessian of \mathcal{L} , which is required to implement a Newton scheme, is given (in abbreviated form) by

$$\text{Hess } \mathcal{L} = \begin{pmatrix} \partial_X^2 \mathcal{E}_{\text{out}} - \partial_X^2 \partial_Y \mathcal{E}_{\text{in}}(P) & \partial_X \partial_Y \mathcal{E}_{\text{out}} - \partial_X \partial_Y^2 \mathcal{E}_{\text{in}}(P) & -\partial_X \partial_Y \mathcal{E}_{\text{in}} \\ \partial_X \partial_Y \mathcal{E}_{\text{out}} - \partial_X \partial_Y^2 \mathcal{E}_{\text{in}}(P) & \partial_Y^2 \mathcal{E}_{\text{out}} - \partial_Y^3 \mathcal{E}_{\text{in}}(P) & -\partial_Y^2 \mathcal{E}_{\text{in}} \\ -\partial_X \partial_Y \mathcal{E}_{\text{in}} & -\partial_Y^2 \mathcal{E}_{\text{in}} & 0 \end{pmatrix}.$$

The different terms in Hess \mathcal{L} are evaluated as follows:

$$\begin{aligned}\partial_X^2 \mathcal{E}_{\text{out}}(\Theta, \Psi) &= \partial_Z^2 \mathbf{M}_\gamma[X - X^k, X^k](\Theta, \Psi) + \frac{\tau}{\tilde{\tau}^2} (\partial_X^2 \mathbf{M}_\gamma[Y - X, X](\Theta, \Psi) \\ &\quad - 2\partial_Z \partial_X \mathbf{M}_\gamma[Y - X, X](\Theta, \Psi) + \partial_Z^2 \mathbf{M}_\gamma[Y - X, X](\Theta, \Psi)), \\ \partial_Y \partial_X \mathcal{E}_{\text{out}}(\Theta, \Psi) &= \frac{\tau}{\tilde{\tau}^2} (\partial_Z \partial_X \mathbf{M}_\gamma[Y - X, X](\Theta, \Psi) - \partial_Z^2 \mathbf{M}_\gamma[Y - X, X](\Theta, \Psi)), \\ \partial_Y^2 \mathcal{E}_{\text{out}}(\Theta, \Psi) &= \frac{\tau}{\tilde{\tau}^2} \partial_Z^2 \mathbf{M}_\gamma[Y - X, X](\Theta, \Psi), \\ \partial_X^2 \partial_Y \mathcal{E}_{\text{in}}(\Theta, \Psi, \Xi) &= \partial_Z^3 \mathbf{M}_\gamma[Y - X, X](\Theta, \Psi, \Xi) - \partial_X \partial_Z^2 \mathbf{M}_\gamma[Y - X, X](\Theta, \Psi, \Xi) \\ &\quad - \partial_X \partial_Z^2 \mathbf{M}_\gamma[Y - X, X](\Theta, \Xi, \Psi) + \partial_X^2 \partial_Z \mathbf{M}_\gamma[Y - X, X](\Theta, \Psi, \Xi), \\ \partial_X \partial_Y^2 \mathcal{E}_{\text{in}}(\Theta, \Psi, \Xi) &= -\partial_Z^3 \mathbf{M}_\gamma[Y - X, X](\Theta, \Psi, \Xi) + \partial_X \partial_Z^2 \mathbf{M}_\gamma[Y - X, X](\Theta, \Psi, \Xi), \\ \partial_Y^3 \mathcal{E}_{\text{in}}(\Theta, \Psi, \Xi) &= \partial_Z^3 \mathbf{M}_\gamma[Y - X, X](\Theta, \Psi, \Xi) + 2\tilde{\tau} \partial_Y^3 \mathbf{A}_\gamma[Y](\Theta, \Psi, \Xi).\end{aligned}$$

In the implementation of the proposed scheme it is convenient to directly treat the squared, dual anisotropy $\gamma^{*,2}(\cdot) := (\gamma^*(\cdot))^2$ in the calculation of derivatives of the anisotropic functionals, which is particularly advantageous for anisotropies of the type $\gamma(p) = \sum_{k=1}^K \sqrt{p \cdot G_k p}$ where the G_k are symmetric and positive definite (cf. Garcke et al. [3]). The different terms of the gradient $\text{grad } \mathcal{L}$ and the Hessian $\text{Hess } \mathcal{L}$ are in the usual way assembled from local contribution on simplices of the polygonal mesh. The required formulas are given in the Appendix.

6 Numerical results

In this section, we show applications of the proposed algorithm to the evolution of curves in \mathbb{R}^2 under anisotropic Willmore flow. Beside anisotropies with ellipsoidal Wulff shapes we study regularized crystalline anisotropies $\gamma(\cdot) = \|\cdot\|_{\ell^1}$ and $\gamma(\cdot) = \|\cdot\|_{\ell^\infty}$ based on a suitable regularization. A particular emphasis is on the verification of the robustness and stability of the proposed approach in particular for large time steps. Furthermore, we experimentally verify that Wulff shapes grow self-similar in time under the corresponding anisotropic Willmore flow.

At first, we study anisotropies of the type

$$\gamma(z) = \sqrt{a_1^2 z_1^2 + a_2^2 z_2^2}$$

for given $a_1, a_2 > 0$. In that case the squared dual anisotropy function is given by

$$\gamma^{*,2}(z) = \frac{z_1^2}{a_1^2} + \frac{z_2^2}{a_2^2}.$$

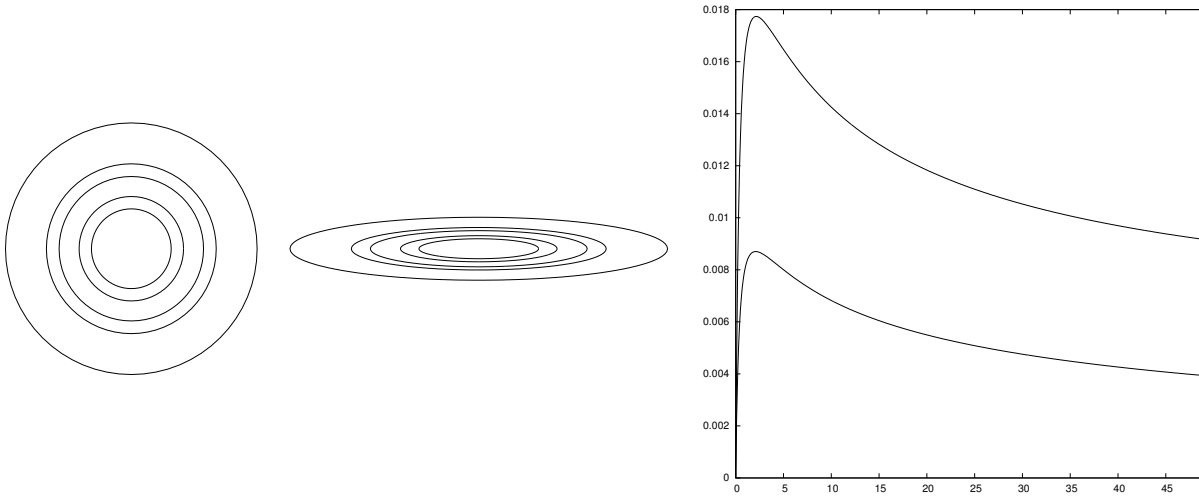


Figure 1: The evolution of an unit circle under isotropic Willmore flow is plotted on the left. For the computation we used as initial grid size $h = 0.0981$ resulting from 64 vertices. Furthermore, $\tau = h$, $\tilde{\tau} = h^2$ and the resulting discrete curves are shown for $t = 0, 10\tau, 50\tau, 100\tau, 500\tau$. In the middle we display the evolution of an ellipse (with half axes 6 and 1) under anisotropic Willmore flow with 256 elements and $h = 0.0984$. Here, we consider $\tau = h$, $\tilde{\tau} = h^2$ and display the approximate solutions for $t = 0, 10\tau, 50\tau, 100\tau, 500\tau$. Next, the associated L^2 -errors are plotted over time on the right, where the lower error curve corresponds to the evolution results on the left.

Figure 1 compares the evolution of a circle of radius $R_0 = 1$ under isotropic Willmore flow for $a_1 = a_2 = 1$ with the evolution of an ellipse with half axes $a_1 = 6$ and $a_2 = 1$ under the corresponding anisotropic flow. As discussed in Section 2 in both cases the initial curve \mathcal{M}_0 expand in a self-similar fashion, i.e. $\mathcal{M}[x(t)] = R(t)\mathcal{M}_0$ with $R(t) = \sqrt[4]{R_0^4 + 2t}$ for $r_0 > 0$. In Figure 1 we plot the evolution of the error $err(h) := \|\mathcal{I}_h x(t) - x_h(t)\|_{L^2}$ in time. Thereby, the L^2 -error is evaluated on the polygonal curve $x_h(t)$ and \mathcal{I}_h denotes the nodal interpolation of $x(t)$ at the projected positions of the nodes of $x_h(t)$ in direction $\nabla\gamma(n[x_h(t)])$. In Table 1 and 2 we provide results on the experimental order of convergence $eoc := \log(err(h_1)/err(h_2))/\log(h_1/h_2)$ for varying grid and time step size in case of the evolution of the circle and the ellipse.

Now, we want to study crystalline anisotropies $\gamma(\cdot) = \|\cdot\|_{\ell^1}$ and $\gamma(\cdot) = \|\cdot\|_{\ell^\infty}$. As already pointed out, even though the formulation of the scheme itself doesn't explicitly need assumptions on the smoothness of γ , the application of the optimization algorithm requires the computation of derivatives of γ up to order 3. In fact, we use the following regularization: For a small parameter $\varepsilon > 0$ we regularize the ℓ^1 -norm by

$$\ell_\varepsilon^1(z) = \sum_{l=1}^2 \sqrt{\varepsilon|z|^2 + z_l^2}.$$

Since in \mathbb{R}^2 the ℓ^∞ -norm equals a rotated and scaled ℓ^1 -norm we use as regularization of the ℓ^∞ -norm

$$\ell_\varepsilon^\infty(z) = \frac{\sqrt{\varepsilon|z|^2 + (z_1 + z_2)^2}}{2} + \frac{\sqrt{\varepsilon|z|^2 + (z_1 - z_2)^2}}{2}.$$

Figure 2 shows the evolution of a sphere with respect to the regularized ℓ^∞ -norm under the associated anisotropy Willmore flow with anisotropy $\gamma(\cdot) = \|\cdot\|_{\ell_\varepsilon^1}$ for $\varepsilon = 0.0001$. Results

n	$h(t)$	L^2 -error ($\tau = \tilde{\tau} = h_0^2$)	<i>eoc</i>	$h(t)$	L^2 -error ($\tau = \tilde{\tau} = h_0$)	<i>eoc</i>
4	4.166e-1	4.830e-3		4.482e-1	1.916e-2	
5	2.096e-1	1.328e-3	1.879	2.258e-1	1.087e-2	0.826
6	1.049e-1	3.403e-4	1.969	1.132e-1	5.804e-3	0.909
7	5.249e-2	8.561e-5	1.992	5.668e-2	3.000e-3	0.954
8	2.625e-2	2.144e-5	1.998	2.836e-2	1.525e-3	0.977

Table 1: The L^2 -error between the exact solution of the self-similar evolution of circles under Willmore flow and the discrete solution of the fully implicit variational time discretization is plotted at time $t = 0.1542$ for a grid size $h(t)$ (left) and $t = 0.3927$ (right). On the left we consider time step sizes τ and $\tilde{\tau}$ of the order of the squared spatial grid size h_0 at the initial time 0, whereas on the right both time step sizes are taken equal to the grid size. In both cases we have considered 2^n vertices for the polygon, resulting in an initial grid size $h_0 = \frac{2\pi}{2^n}$.

n	$h(t)$	L^2 -error ($\tau = \tilde{\tau} = h_0^2$)	<i>eoc</i>	$h(t)$	L^2 -error ($\tau = \tilde{\tau} = h_0$)	<i>eoc</i>
5	1.435e+0	1.648e-1		1.274e+0	1.942e-1	
6	6.487e-1	3.476e-2	1.960	5.875e-1	7.089e-2	1.303
7	3.069e-1	8.762e-3	1.841	2.842e-1	3.424e-2	1.002
8	1.525e-1	2.182e-3	1.987	1.396e-1	1.724e-3	0.966

Table 2: As in Table 1 experimental orders of convergence are reported, now for the self-similar evolution of the ellipses (with half axis 6 and 1) under anisotropic Willmore flow. Here, again polygons with 2^n vertices are considered, equi-distributed along the initial ellipse with an initial grid size $h_0 = \frac{24.172}{2^n}$. On the left the error is evaluated at time $t = 0.596576$ and on the right at time $t = 0.77238$.

on the self similar evolution of spheres with respect to the regularized ℓ^1 -norm are depicted in Figure 3. In these simulations, we use the analog regularization for the dual anisotropy γ^* required in the algorithm.

Next, we generalize Willmore flow and replace the Willmore energy by the modified energy

$$e_\gamma[x] := \int_{\mathcal{M}[x]} \left(\frac{1}{2} \mathbf{h}_\gamma^2 + \lambda \right) \gamma(n[x]) da, \quad (6.1)$$

with a second term given by the anisotropic area weighted with a constant $\lambda > 0$. The incorporation of this generalized energy in our computational approach is straightforward. The generalized flow combines expansive forcing with respect to the anisotropic Willmore flow of curves with contractive forcing due to the anisotropic mean curvature motion associated to the anisotropic area functional. Thus, for the generalized model we expect convergence to a limit shape given by a scaled Wulff shape, where the scaling depends on the factor λ . Fig. 4 shows the impact of the factor λ on the evolution, whereas in Fig. 5 we compare the evolution of different initial shapes under the generalized anisotropic Willmore flow for different anisotropies.

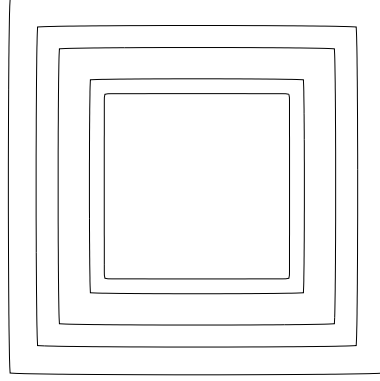


Figure 2: Evolution of the unit sphere with respect to the regularized ℓ^∞ -norm under anisotropic Willmore flow for the anisotropy $\|\cdot\|_{\ell_\varepsilon^1}$ with $\varepsilon = 0.0001$. For this computation we consider 200 vertices leading to an initial grid size $h_0 = 0.04$. Furthermore, $\tau = h_0$ and $\tilde{\tau} = h_0^2$ and the resulting discrete curves are shown for $t = 0, 10\tau, 50\tau, 100\tau, 200\tau$.

Appendix

Here, we collect the computational ingredients to evaluate the Lagrangian, its gradient and Hessian based on a standard local assembly procedure. In the following for vectors $x \in \mathbb{R}^{d+1}$ and functions f we use the notation $f_{i,j}(x) = \frac{\partial f_i(x)}{\partial x_j}$ and in analogy for higher order derivatives. Furthermore, for matrices A we use $f_{k,ij}(A) = \frac{\partial f_k(A)}{\partial A_{ij}}$ and again in analogy for higher order derivatives. In fact, we can restrict ourselves to the local functionals

$$\mathbf{M}_{T,\gamma}[Z, X] = \frac{1}{(d+1)!} \left(\sum_{i=0, \dots, d} \gamma^*(\bar{Z}_i)^2 \right) \gamma(R[\bar{X}]), \quad \mathbf{A}_{T,\gamma}[X] = \frac{1}{d!} \gamma(R[\bar{X}]), \quad (6.2)$$

where we denote by $\bar{Z} = (Z_0, \dots, Z_d)$ and $\bar{X} = (X_0, \dots, X_d)$ the corresponding vectors of simplex nodes in \mathbb{R}^{d+1} with coordinate representation $Z_j = (Z_{jr})_{r=1, \dots, d+1}$ and $X_j = (X_{jr})_{r=1, \dots, d+1}$. Here, R is a mapping from $\mathbb{R}^{(d+1)^2}$ to \mathbb{R}^{d+1} representing the 90° rotated edge vector for $d = 1$ and the cross product of edge vectors for $d = 2$, respectively. For $d = 1$ we obtain for the first derivatives of $R[\bar{X}] = \begin{pmatrix} X_{02} - X_{12} \\ X_{11} - X_{01} \end{pmatrix}$ with respect to the entries (ij) with $i = 0, \dots, d$ and $j = 1, \dots, d+1$

$$R_{,01}[\bar{X}] = \begin{pmatrix} 0 \\ -1 \end{pmatrix}, \quad R_{,02}[\bar{X}] = \begin{pmatrix} 1 \\ 0 \end{pmatrix}, \quad R_{,11}[\bar{X}] = \begin{pmatrix} 0 \\ 1 \end{pmatrix}, \quad R_{,12}[\bar{X}] = \begin{pmatrix} -1 \\ 0 \end{pmatrix}.$$

Because of the linearity of R for $d = 1$ all higher derivatives vanish. For $d = 2$ we have

$$R[\bar{X}] = \left(\sum_{u,v=1}^3 \epsilon_{iuv} (X_{1u} - X_{0u})(X_{2v} - X_{0v}) \right)_{i=1,2,3},$$

where ϵ_{wuv} is the Levi-Civita symbol ($\epsilon_{wuv} = \pm 1$ if (w, u, v) is a even/odd permutation of $(1, 2, 3)$ and 0 else). Thus, for $w = 1, 2, 3$ we have

$$R_{w,js}[\bar{X}] = \sum_{u,v=1}^3 \epsilon_{wuv} ((\delta_{1j} - \delta_{0j})\delta_{su}(X_{2v} - X_{0v}) + (\delta_{2j} - \delta_{0j})\delta_{sv}(X_{1u} - X_{0u})),$$

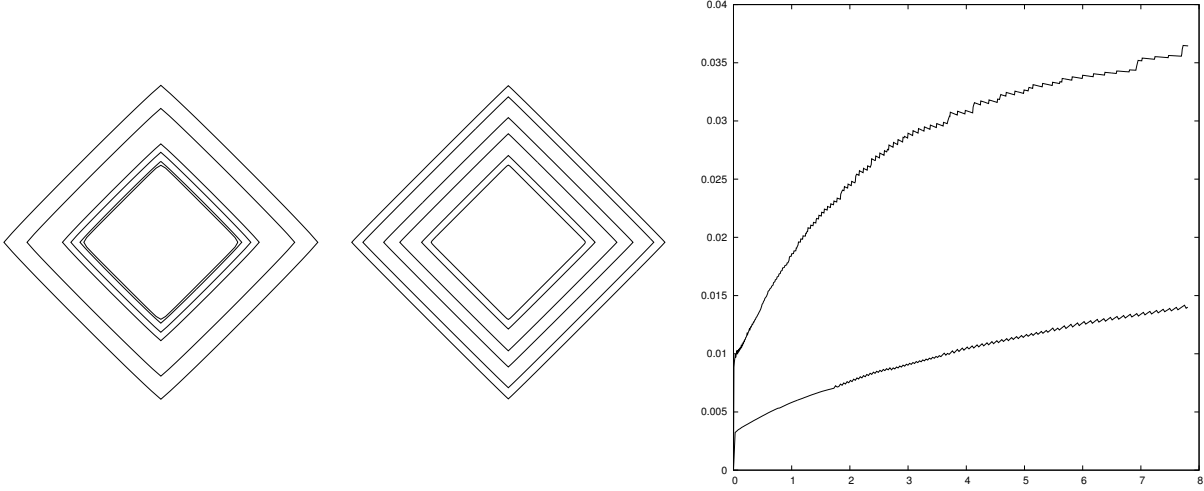


Figure 3: Evolution of the unit sphere with respect to the regularized ℓ^1 -norm under anisotropic Willmore flow for the anisotropy $\gamma(\cdot) = \|\cdot\|_{\ell^\infty}$. The parameters are $h_0 = 0.0078$, $\varepsilon = 0.001$, $\tau = \tilde{\tau} = h_0^2$ and curves are plotted at times $t = 0, 10\tau, 50\tau, 100\tau, 500\tau, 1000\tau$ on the left and $h_0 = 0.0283$, $\varepsilon = 0.0001$, $\tau = h_0$, $\tilde{\tau} = h_0^2$, $t = 0, 10\tau, 50\tau, 100\tau, 200\tau, 275\tau$ in the middle. On the right the associated L^2 -errors are plotted over time, where the lower error curve corresponds to the evolution results on the left.

$$R_{w,jslt}[\bar{X}] = \sum_{u,v=1}^3 \epsilon_{wuv} ((\delta_{1j} - \delta_{0j})(\delta_{2l} - \delta_{0l})\delta_{su}\delta_{tv} + (\delta_{2j} - \delta_{0j})(\delta_{1l} - \delta_{0l})\delta_{sv}\delta_{tu}),$$

and all third derivatives $R_{u,irjslt}[\bar{X}]$ vanish. Here $j, l \in \{0, 1, 2\}$ refer to the local node and $s, t \in \{1, 2, 3\}$ to the spacial component. Next we derive expressions for the derivatives of (4.3) and (4.4) under the assumption that γ, γ^* are sufficiently smooth in $\mathbb{R}^{d+1} \setminus \{0\}$ (thus $Z_i, R[\bar{X}] \neq 0$):

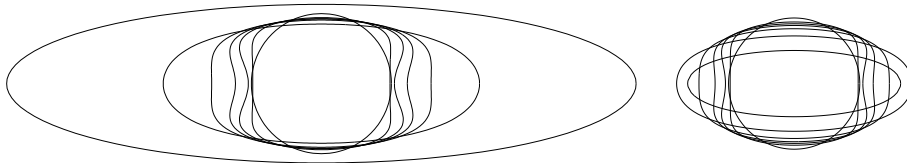


Figure 4: The impact of the parameter λ is shown for the evolution of a circle to an ellipse with aspect ratio 4 : 1 (i.e. $a_1 = 4$ and $a_2 = 1$). We evolve polygons with 160 vertices approximating the unit sphere as initial curve, $h_0 = 0.0393$ and $\tau = \tilde{\tau} = 0.01$, $h = 0.000393$. On the left $\lambda = 0.025$ and on the right $\lambda = 4$.

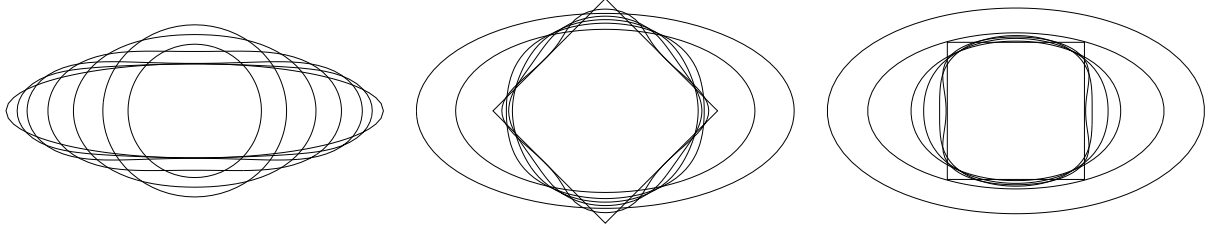


Figure 5: The evolution of different initial shapes for different anisotropies is displayed. For all computations we use 100 vertices and choose $\lambda = 0.25$. On the left we start with an ellipse with aspect ratio 4 : 1 under an isotropic flow with $\gamma(\cdot) = \|\cdot\|$ ($h_0 = 0.1739$, $\tau = h_0$, $\tilde{\tau} = h_0^2$) results are shown at $t = 0, 0.1739, 0.5218, 1.739, 3.478, 6.956, 173.9$. In the middle and on the right an ellipsoidal anisotropy with aspect ratio 2 : 1 is used (i.e. $a_1 = 2$, $a_2 = 1$) in the first case (middle), we take as initial shape the unit sphere for the l^1 -norm ($h_0 = 0.0566$, $\tau = \tilde{\tau} = 0.001 h_0$) and results are displayed at $t = 0, 0.00017, 0.00085, 0.00169, 0.006, 0.056, 0.251$. In the second example (right), the initial shape is the unit sphere for the l^∞ -norm ($h_0 = 0.08$ and $\tau = \tilde{\tau} = 0.01 h_0$) and results are depicted for $t = 0, 0.0024, 0.008, 0.04, 0.08, 0.8, 4.8$.

Derivatives of $\mathbf{M}_{T,\gamma}$

$$\begin{aligned}
 \partial_{Z_{ir}} \mathbf{M}_{T,\gamma}[Z, X] &= \frac{1}{(d+1)!} \gamma_{,r}^{*,2}(Z_i) \gamma(R[\bar{X}]), \\
 \partial_{Z_{js}} \partial_{Z_{ir}} \mathbf{M}_{T,\gamma}[Z, X] &= \frac{\delta_{ij}}{(d+1)!} \gamma_{,rs}^{*,2}(Z_i) \gamma(R[\bar{X}]), \\
 \partial_{Z_{it}} \partial_{Z_{js}} \partial_{Z_{ir}} \mathbf{M}_{T,\gamma}[Z, X] &= \frac{\delta_{ij} \delta_{il}}{(d+1)!} \gamma_{,rst}^{*,2}(Z_i) \gamma(R[\bar{X}]), \\
 \partial_{X_{ir}} \mathbf{M}_{T,\gamma}[Z, X] &= \frac{1}{(d+1)!} \left(\sum_{\alpha=0,\dots,d} \gamma^{*,2}(\bar{Z}_\alpha) \right) \sum_{s=1}^m \gamma_{,s}(R[\bar{X}]) R_{s,ir}[\bar{X}], \\
 \partial_{X_{js}} \partial_{X_{ir}} \mathbf{M}_{T,\gamma}[Z, X] &= \frac{1}{(d+1)!} \left(\sum_{\alpha=0,\dots,d} \gamma^{*,2}(\bar{Z}_\alpha) \right) \\
 &\quad \cdot \left(\sum_{t=1}^m \gamma_{,t}(R[\bar{X}]) R_{t,ir} R_{t,js}[\bar{X}] + \sum_{t,u=1}^m \gamma_{,tu}(R[\bar{X}]) R_{t,ir}[\bar{X}] R_{u,js}[\bar{X}] \right), \\
 \partial_{X_{js}} \partial_{Z_{ir}} \mathbf{M}_{T,\gamma}[Z, X] &= \frac{1}{(d+1)!} \gamma_{,r}^{*,2}(Z_i) \sum_{t=1}^m \gamma_{,t}(R[\bar{X}]) R_{t,js}[\bar{X}], \\
 \partial_{X_{it}} \partial_{Z_{js}} \partial_{Z_{ir}} \mathbf{M}_{T,\gamma}[Z, X] &= \frac{\delta_{ij}}{(d+1)!} \gamma_{,rs}^{*,2}(Z_i) \sum_{u=1}^m \gamma_{,u}(R[\bar{X}]) R_{u,it}[\bar{X}], \\
 \partial_{X_{it}} \partial_{X_{js}} \partial_{Z_{ir}} \mathbf{M}_{T,\gamma}[Z, X] &= \frac{1}{(d+1)!} \gamma_{,r}^{*,2}(Z_i)
 \end{aligned}$$

$$\cdot \left(\sum_{v=1}^m \gamma_{,v}(R[\bar{X}])R_{v,js}R_{lt}[\bar{X}] + \sum_{v,u=1}^m \gamma_{,vu}(R[\bar{X}])R_{v,js}[\bar{X}]R_{u,lt}[\bar{X}] \right),$$

Derivatives of $\mathbf{A}_{T,\gamma}$

$$\begin{aligned} \partial_{Y_{ir}} \mathbf{A}_{T,\gamma}[X] &= \frac{1}{d!} \sum_{s=1}^m \gamma_{,s}(R[\bar{X}])R_{s,ir}[\bar{X}], \\ \partial_{Y_{js}} \partial_{Y_{ir}} \mathbf{A}_{T,\gamma}[X] &= \frac{1}{d!} \left(\sum_{t=1}^m \gamma_{,t}(R[\bar{X}])R_{t,ir}R_{js}[\bar{X}] + \sum_{t,u=1}^m \gamma_{,tu}(R[\bar{X}])R_{t,ir}[\bar{X}]R_{u,js}[\bar{X}] \right), \\ \partial_{Y_{lt}} \partial_{Y_{js}} \partial_{Y_{ir}} \mathbf{A}_{T,\gamma}[X] &= \frac{1}{d!} \left(\sum_{u,v=1}^m \gamma_{,vu}(R[\bar{X}])R_{v,ir}R_{js}[\bar{X}]R_{u,lt}[\bar{X}] + \sum_{v=1}^m \gamma_{,v}(R[\bar{X}])R_{v,ir}R_{js}R_{lt}[\bar{X}] \right. \\ &\quad + \sum_{u,v,w=1}^m \gamma_{,vuw}(R[\bar{X}])R_{v,ir}[\bar{X}]R_{u,js}[\bar{X}]R_{w,lt}[\bar{X}] \\ &\quad \left. + \sum_{u,v=1}^m \gamma_{,vu}(R[\bar{X}])R_{v,ir}R_{lt}[\bar{X}]R_{u,js}[\bar{X}] + \sum_{u,v=1}^m \gamma_{,vu}(R[\bar{X}])R_{v,ir}[\bar{X}]R_{u,js}R_{lt}[\bar{X}] \right). \end{aligned}$$

Acknowledgement.

Ricardo Perl was supported by the DFG project Ru 567/14-1 and Martin Rumpf acknowledges support by the SFB 611.

References

- [1] N. Balzani and M. Rumpf. A nested variational time discretization for parametric Willmore flow. *Interfaces and Free Boundaries*, 14(4):431–454, 2012.
- [2] J. W. Barrett, H. Garcke, and R. Nürnberg. A parametric finite element method for fourth order geometric evolution equations. *J. Comp. Phys.*, 222:441–467, 2007.
- [3] J. W. Barrett, H. Garcke, and R. Nürnberg. Numerical approximation of anisotropic geometric evolution equations in the plane. *IMA Journal of Numerical Analysis*, 28(2):292–330, 2008.
- [4] J. W. Barrett, H. Garcke, and R. Nürnberg. Parametric approximation of isotropic and anisotropic elastic flow for closed and open curves. *Num. Math.*, 120:489 – 542, 2012.
- [5] G. Bellettini. Anisotropic and crystalline mean curvature flow. In D. Bao, R. L. Bryant, S.-S. Chern, and Z. Shen, editors, *A Sampler of Riemann-Finsler geometry*, volume 50, pages 49–82. Cambridge Univ. Press, 2004.
- [6] G. Bellettini, V. Caselles, A. Chambolle, and M. Novaga. Crystalline mean curvature flow of convex sets. *Archive for Rational Mechanics and Analysis*, 179(1):109–152, 2006.
- [7] G. Bellettini and L. Mugnai. Anisotropic geometric functionals and gradient flows. *Banach Center Publications*, 86:21–43, 2009.

- [8] M. Bertalmio, A. Bertozzi, and G. Sapiro. Navier-stokes, fluid dynamics, and image and video inpainting. In *IEEE Proceedings of the International Conference on Computer Vision and Pattern Recognition*, volume 1, pages 355–362, 2001.
- [9] M. Bertalmio, G. Sapiro, V. Caselles, and C. Ballester. Image inpainting. In *Proc. of SIGGRAPH 2000*, pages 417–424, New Orleans, USA, July 2000.
- [10] I. A. Bobenko and P. Schröder. Discrete Willmore flow. pages 101–110. ACM Press, 2005.
- [11] A. Chambolle. An algorithm for mean curvature motion. *Interfaces and free Boundaries*, 6:195–218, 2004.
- [12] A. Chambolle and M. Novaga. Convergence of an algorithm for anisotropic mean curvature motion. *SIAM J. Math. Anal.*, 37:1978–1987, 2006.
- [13] T. F. Chan, S. H. Kang, and J. Shen. Euler’s elastica and curvature-based inpainting. *SIAM Appl. Math.*, 63(2):564–592, 2002.
- [14] U. Clarenz. Enclosure theorems for extremals of elliptic parametric functionals. *Calculus of Variations*, 15:313–324, 2002.
- [15] U. Clarenz. The Wulff-shape minimizes an anisotropic Willmore functional. *Interfaces and Free Boundaries*, 6(3):351–359, 2004.
- [16] U. Clarenz, U. Diewald, G. Dziuk, M. Rumpf, and R. Rusu. A finite element method for surface restoration with smooth boundary conditions. *Computer Aided Geometric Design*, 21(5):427–445, 2004.
- [17] U. Clarenz, G. Dziuk, and M. Rumpf. On generalized mean curvature flow in surface processing. In H. Karcher and S. Hildebrandt, editors, *Geometric analysis and nonlinear partial differential equations*, pages 217–248. Springer, 2003.
- [18] K. Deckelnick and G. Dziuk. Error analysis of a finite element method for the Willmore flow of graphs. *Interfaces and Free Boundaries*, 8:21–46, 2006.
- [19] K. Deckelnick and G. Dziuk. Error analysis for the elastic flow of parametrized curves. *Math. Comp.*, 78(266):645–671, 2009.
- [20] K. Deckelnick and F. Schieweck. Error analysis for the approximation of axisymmetric willmore flow by c_1 -elements. *Interfaces and Free Boundaries*, 12(4):551–574, 2010.
- [21] U. Diewald. *Anisotrope Krümmungsflüsse parametrischer Flächen sowie deren Anwendung in der Flächenverarbeitung*. Dissertation, University Duisburg, 2005.
- [22] M. Droske. *On Variational Problems and Gradient Flows in Image Processing*. Dissertation, University Duisburg, 2005.
- [23] M. Droske and M. Rumpf. A level set formulation for Willmore flow. *Interfaces and Free Boundaries*, 6(3):361–378, 2004.
- [24] Q. Du, C. Liu, and X. Wang. Simulating the deformation of vesicle membranes under elastic bending energy in three dimensions. *Journal of Computational Physics*, 212(2):757–777, 2006.
- [25] G. Dziuk. Finite elements for the Beltrami operator on arbitrary surfaces. In S. Hildebrandt and R. Leis, editors, *Partial Differential Equations and Calculus of Variations*, Lecture Notes in Mathematics 1357, pages 142–155. Springer, 1988.
- [26] G. Dziuk. An algorithm for evolutionary surfaces. *Numer. Math.*, 58:603–611, 1991.

- [27] G. Dziuk. Convergence of a semi-discrete scheme for the curve shortening flow. *Mathematical Models and Methods in Applied Sciences*, 4:589–606, 1994.
- [28] G. Dziuk. Discrete anisotropic curve shortening flow. *Siam J. Numer. Anal.*, 36(6):1808–1830, 1999.
- [29] W. Helfrich. Elastic properties of lipid bilayers: Theory and possible experiments. *Zeitschrift für Naturforschung*, 28c:693–703, 1973.
- [30] E. Kuwert and R. Schätzle. The Willmore flow with small initial energy. *J. Differential Geom.*, 57(3):409–441, 2001.
- [31] E. Kuwert and R. Schätzle. Gradient flow for the Willmore functional. *Comm. Anal. Geom.*, 10(5):1228–1245 (electronic), 2002.
- [32] S. Luckhaus and T. Sturzenhecker. Implicit time discretization for the mean curvature flow equation. *Calc. Var.*, 3:253–271, 1995.
- [33] U. Mayer and G. Simonett. A numerical scheme for axisymmetric solutions of curvature driven free boundary problems with applications to the Willmore flow. *Interphases and Free Boundaries*, 4(1):89–109, 2002.
- [34] D. Mumford. Elastica and computer vision. In C. Bajaj, editor, *Algebraic Geometry and Its Applications*, pages 491–506. Springer, New York, 1994.
- [35] O. Nemitz. *Anisotrope Verfahren in der Bildverarbeitung: Gradientenflüsse, Level-Sets und Narrow Bands*. Dissertation, University of Bonn, 2008.
- [36] M. Nitzberg, D. Mumford, and T. Shiota. *Filtering, Segmentation and Depth (Lecture Notes in Computer Science Vol. 662)*. Springer-Verlag Berlin Heidelberg, 1993.
- [37] J. Nocedal and S. J. Wright. *Numerical Optimization*. Springer, New York / Berlin, 1999.
- [38] N. Olischläger and M. Rumpf. Two step time discretization of Willmore flow. In E. R. Hancock, R. R. Martin, and M. A. Sabin, editors, *IMA Conference on the Mathematics of Surfaces*, volume 5654 of *Lecture Notes in Computer Science*, pages 278–292. Springer, 2009.
- [39] B. Palmer. Equilibria for anisotropic bending energies. *Math. Phys.*, 50(2):023512, 2009.
- [40] A. Polden. Closed Curves of Least Total Curvature. *SFB 382 Tübingen, Preprint*, 13, 1995.
- [41] A. Polden. Curves and Surfaces of Least Total Curvature and Fourth-Order Flows. *Dissertation, Universität Tübingen*, page , 1996.
- [42] P. Pozzi. On the gradient flow for the anisotropic area functional. *Math. Nachr.*, 285:707–726, 2012.
- [43] T. Rivière. Analysis aspects of Willmore surfaces. *Invent. Math.*, 174(1):1–45, 2008.
- [44] R. Rusu. An algorithm for the elastic flow of surfaces. *Interfaces and Free Boundaries*, 7:229–239, 2005.
- [45] R. Schaback and H. Wendland. *Numerische Mathematik*. Springer, 5. edition, 2004.
- [46] U. Seifert. Configurations of fluid membranes and vesicles. *Advances in Physics*, 46:13–137, 1997.
- [47] G. Simonett. The Willmore Flow near spheres. *Diff. and Integral Eq.*, 14(8):1005–1014, 2001.

- [48] W. Welch and A. Witkin. Variational surface modeling. *Computer Graphics*, 26(2):157–166, 1992.
- [49] T. Willmore. *Riemannian Geometry*. Clarendon Press, Oxford, 1993.
- [50] G. Xu and Q. Pan. G^1 surface modelling using fourth order geometric flows. *Computer-Aided Design*, 38(4):392–403, 2006.
- [51] S. Yoshizawa and A. G. Belyaev. Fair triangle mesh generation with discrete elastica. In *Proceedings of the Geometric Modeling and Processing: Theory and Applications (GMP'02)*, pages 119–123, Washington, DC, USA, 2002. IEEE Computer Society.